Binding of curcumin with glyoxalase I: Molecular docking, molecular dynamics simulations, and kinetics analysis

Ming Liu, Minggui Yuan, Minxian Luo, Xianzhang Bu, Hai-Bin Luo *, Xiaopeng Hu *

School of Pharmaceutical Sciences, Sun Yat-Sen University, Guangzhou 510006, PR China

A B S T R A C T

Glyoxalase I (GLOI) is a key metalloenzyme in glycolytic pathway by detoxifying reactive α-ketoaldehydes such as methylglyoxal. Recent studies demonstrate that the nature product curcumin is an efficient inhibitor of GLOI, but its binding mechanism towards GLOI is still unclear. In the present study, molecular docking and molecular dynamics (MD) simulations were performed to better understand the inhibitory mechanism of curcumin towards GLOI. The enol form of curcumin coordinates with the catalytic zinc ion of GLOI and forms a strong hydrogen bond with Glu 172, whereas its keto tautomer displays unfavorable electrostatic interactions with Glu 172 and Glu 99. The calculated binding free energies suggest that GLOI prefers the primary enol form ($\Delta G = -30.38$ kcal/mol) to the keto tautomer ($\Delta G = -24.16$ kcal/mol). The present work also reveals that bisdemethoxycurcumin binds to GLOI in a similar manner as curcumin and exhibits a slightly less negative predicted binding free energy, which is further validated by our comparative kinetics analysis ($Ki = 18.2$ and 10.3 μM for bisdemethoxycurcumin and curcumin, respectively). Results of the study can provide an insight into the development of novel and more effective GLOI inhibitors.

1. Introduction

The glyoxalase system is a ubiquitous detoxification pathway that protects against cellular damage caused by highly reactive oxoaldehydes like methylglyoxal, which is mainly formed as a by-product of glycolysis [1]. The system consists of two metalloenzymes, glyoxalase I (GLOI) (EC 4.4.1.5) and glyoxalase II (GLOII) (EC 3.1.2.6). GLOI catalyzes the isomerization of the thiohemiacetal of glutathione and a 2-oxoaldehyde into the thiolester of GSH and the corresponding 2-hydroxycarboxylic acid, respectively [1–4]. Since high activities of GLOI have been reported in tumor tissues, inhibitors of GLOI can increase the accumulation of methylglyoxal, and result in significant anti-tumor activity in vitro and in vivo studies [5–9]. Hence, GLOI is receiving considerable attention as a potential target for anti-tumor drugs in recent years [10,11].

Great efforts have been made to design and synthesize structure-based and mechanism-based inhibitors of GLOI. Most of them, if not all, are derivatives of glutathione as mimics of the substrate of GLOI. Unfortunately, the structural similarity of these inhibitors to glutathione made them extremely labile as substrates of other enzymes such as γ-GT. Although this problem could be resolved by structural scaffolding modifications (e.g., isosteric replacements for thiohydroxamate linkage), the developing glutathione derivatives as drug leads still have a major obstacle due to their charged glutathionyl functional group which preventing rapid diffusion into cells [10,11].

Curcumin is a natural polyphenol derived from the plant *Curcuma longa*, which has been used in the Indian Ayurveda medicine. Extensive researches reveal that curcumin exhibits a remarkable range of pharmacological activities, such as anti-inflammatory, anti-oxidant, anti-viral, and anti-tutor activities [11,12]. Recent research also indicated that these pharmacological actions of curcumin may owe to its inhibition against cellular glyoxalases [13]. Enzyme kinetics studies reveal that curcumin elicits a significant inhibitory activity on GLOI ($Ki = 5.1$ μM) [13].

Curcumin can exist in at least two tautomeric forms, keto and enol (Scheme 1). The latter is energetically more stable in the solid and solution phases due to an intra-molecular hydrogen bonding [14]. By simulating the interaction of flavonoids with GLOI, Takasawa et al. proposed a pharmacophore in which compounds containing a plane configuration of a ketone and a neighbouring hydroxy group in a distance of 2.8 Å may coordinate with the catalytic zinc ion and thus inhibit GLOI [15]. Since the enol form of curcumin possesses a plane configuration with the ketone and hydroxy group arranged at the distance of 2.5 ± 0.5 Å, it is suggested that the enol form could directly interacts with the active site of GLOI [13]. However, no solid evidence has been provided.

Although X-ray crystallography is the most reliable way to analyze the exact interaction of a protein and its ligand, it is not feasible in the case of curcumin and its targeted protein. Curcumin can be photo-bleached, especially by short wavelengths of the light. X-ray diffraction dada collection experiment has shown that on in-house X-ray diffractor, the crystal color of the lipoxygenase–curcumin complex changed from yellow to purple and indicated a radical damage. During the following structure resolution process, an unoccupied electron density, which is

* Corresponding authors. Tel.: +86 20 39943031, +86 20 39943032.
E-mail addresses: luohb77@mail.sysu.edu.cn (H.-B. Luo), huxpeng@mail.sysu.edu.cn (X. Hu).
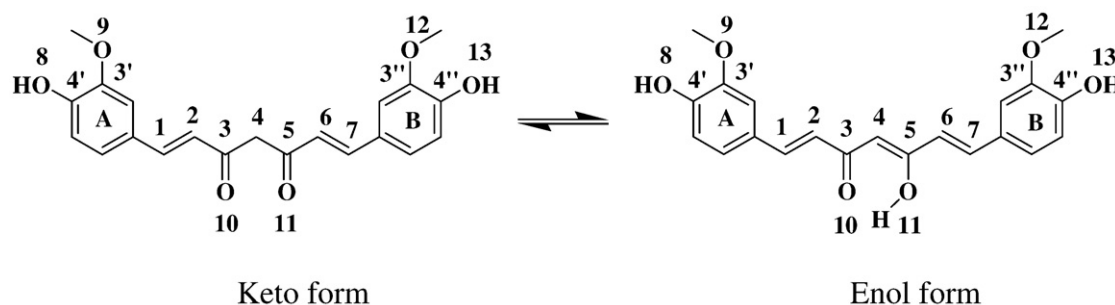
Scheme 1. Two tautomeric forms of curcumin.

smaller than curcumin but its mass is much too large to be a solvent molecule, was found at the active site. Mass spectroscopy analysis further identified potential products of the photo-degradation of curcumin in the X-ray irradiated crystals [16].

To further explore the structural characters of the GLOI/curcumin complexes, molecular docking, molecular dynamics simulations, and MM-PBSA (Molecular Mechanical and Poisson Born/Surface Accessible) binding-free-energy calculations were performed on two GLOI systems in complexes with the keto and enol forms of curcumin. In addition, comparative kinetic analysis on curcumin and its analogue bisdemethoxycurcumin was carried out to qualitatively validate their inhibitory effect as predicted by the binding-free-energy calculations. The present work reveals that GLOI in complex with the enol form could lead to an energy-favorable complex, which may induce the physiological effect. Results of the study not only support the use of curcumin as a potential therapeutic agent by targeting GLOI, also help the development of novel GLOI inhibitors based on curcumin and other natural products.

2. Methods and materials

All calculations in this work were based on the X-ray structure (PDB code 1QIN) of human GLOI in complex with s-(N-hydroxy-N-P-iodophenylcarbamoyl) glutathione (HIPC-GSH) [4]. Hydrogen atoms were added to the system. All ionizable residues were set at their default protonation states at a neutral pH. The metal zinc ion was assigned a charge of $+2$.

2.1. Molecular docking

The docking procedure was carried out using the CDOCKER protocol implemented in Accelrys Discovery Studio 2.1 [17,18]. The ligand-binding site of GLOI was constructed by using HIPC-GSH [4] as a reference ligand. The keto and enol forms of curcumin were docked into the input site sphere, defined with a radius of 10 Å from the centre of the ligand-binding site. A conformational search of each ligand was performed using a simulated annealing molecular dynamics approach. The ligands were heated to a temperature of 700 K in 2000 steps and then annealed to 300 K in 5000 steps. The grid extension was set to 8 Å. Ten random conformations were generated for each ligand. A final minimization step was applied to each ligand docking poses. Residues which located inside the 10 Å interaction sphere were allowed to move during minimization. The docking pose with the lowest binding free energy for each form was selected as the best pose. Two systems were prepared. System 1, named keto complex, is that GLOI is in complex with the keto form of curcumin, while system 2, named enol complex, is that GLOI is in complex with the enol form of curcumin.

2.2. Molecular dynamics (MD) simulations

The AMBER 10 program suite [19] was used to perform all the MD simulations in this study. Based on the electrostatic potential (ESP)

calculations at the *ab initio* HF/6-31G* level [20], the partial atomic charges for each form of curcumin were calculated by using the restricted electrostatic potential (RESP) [21] fitting protocol implemented in the Antechamber module of the AMBER 10 package. The Zn^{2+} ion was treated using the "non-bonded model" method, which only considers the coordination of its adjacent residues in the active site and ligands to zinc as electrostatic and van der Waals forces instead of covalent bonds [22–24]. The electrostatic and van der Waals parameters were obtained from the "parm99.dat" data file of the Amber force field. Each initial model of two complexes was modeled using XleaP module. The AMBER ff03 force field was used as the parameters for GLOI, while the general AMBER force field (GAFF) [21] was used as the parameters for curcumin. The complexes were neutralized by adding sodium counterions, and were solvated in a rectangular box of water molecules with solvent layers 10 Å between the box edges and solute surface.

The two complexes were energy-minimized to remove possible steric stress. The relaxed structures were then subjected to MD simulations. Each complex was gradually heated from 0 to 300 K in 50 ps and then equilibrated for 50 ps at 300 K using the NVT (constant composition, volume, and temperature) ensemble. A weak constraint of 10 kcal mol^{-1}Å^{-2} was employed to keep the protein constrained during the heating procedure. Finally, periodic boundary dynamics simulations of 6 ns were carried out for the production step in an NPT (constant composition, pressure, and temperature) ensemble at 1 atm and 300 K. The temperature was kept at 300 K by means of the weak-coupling algorithm [25]. The SHAKE algorithm [26] was turned on for all bonds involving hydrogens with a tolerance of 1×10^{-5} Å. The Particle–Mesh–Ewald method [27] was applied to treat the long range electrostatic interactions with a 10 Å non-bonded cutoff. The output trajectory files were saved every 1 ps for subsequent analysis. Equilibration was monitored by convergence in terms of the temperature, energy, and density of the system and the root-mean-squared deviations (RMSD) of the backbone atoms compared to the X-ray crystal structure.

2.3. Binding free energy analysis

In the present study, we calculated the binding free energies (ΔG_{bind}) of the receptor/ligand complexes using the MM-PBSA method. MM-PBSA approach, which is encoded in the AMBER 10 program, was applied to compute the binding free energy between a ligand and its targeted protein [28–30]. A grid spacing of 0.5 Å was chosen, and the dielectric constants for the solute and solvent were set to 1 and 80, respectively. The optimized atomic radii set in AMBER 10 were used. A total of 500 snapshots were taken from the last 1 ns trajectory with an interval of 2 ps. All counterions and water molecules were stripped. For each snapshot, a free energy is calculated for each molecular species (complex, receptor, and ligand) and the ligand-binding free energy is calculated by the following equation [30]:

$$\Delta G_{bind} = G_{complex} - [G_{receptor} + G_{ligand}] \tag{1}$$

The binding free energy contains an enthalpic and entropic contribution:

$$\Delta G = \Delta H - T\Delta S \tag{2}$$

The enthalpy of binding ΔH is composed of ΔG_{MM}, the change in the molecular mechanics free energy upon complex formation, ΔG_{solv}, the solvated free energy contribution, and $-T\Delta S$ represents the entropy term. The molecular mechanics free energy is calculated as follows:

$$\Delta G_{MM} = \Delta G_{ele} + \Delta G_{vdw} \tag{3}$$

ΔG_{ele} and ΔG_{vdw} represent the Coulomb and van der Waals interactions, respectively. The solvation free energy is composed of two components.

$$\Delta G_{sol} = \Delta G_{ele,sol} + \Delta G_{nonpol,sol} \tag{4}$$

$\Delta G_{ele,sol}$ is the polar contribution to solvation, and $\Delta G_{nonpol,sol}$ is the nonpolar solvation term. The former could be obtained by solving the Poisson–Boltzmann equation for MM-PBSA method, whereas the latter term was determined using

$$\Delta G_{nonpol,sol} = \gamma\Delta SASA + b \tag{5}$$

where γ, representing the surface tension, and b, being a constant, were set to 0.0072 kcal/(mol Å^2) and 0 [31], respectively. SASA is the solvent accessible surface area (Å^2) that was estimated using the MSMS algorithm with probe radius of 1.4 Å [32].

Normal mode analysis is useful to estimate entropic changes of the solute molecule. However, it is computationally expensive and tends to have a large margin of error that introduces significant uncertainty in the result [30,33]. In this case, different ligands binding to the same protein produce similar entropy. Involving entropy in the calculation would not make much difference for the comparison of the binding free energies of different ligands. So the entropy contribution was not considered because of the similarity of the two forms of curcumin. Therefore, the calculated binding energies herein were not absolute ones, they can only be compared with each other to evaluate the binding affinity with GLOI.

2.4. Enzyme kinetic analysis

Curcumin and bisdemethoxycurcumin (98% purity HPLC) were purchased from Sinopharm Chemical Reagent Co, Ltd. China. Plasmid for 6-His tagged recombinant human GLOI expression was purchased from GeneCopoeia (Germantown Maryland, Catalog no. EX-C0271-B01). Recombinant protein was expressed in the E. coli BL21 (DE3) strain and purified on a HisTrap HP column using FPLC (GE Healthcare) according to the manufacture. Protein concentration was determined using Bradford assay.

Kinetic measurement of GLOI activity was carried out as described previously with minor modification [34]. Generally, formation of S-Dlactoylglutathione was measured by monitoring the increment in absorbance at 240 nm at 30 °C with a thermostated spectrophotometer. Reaction buffer contained 0.10 M sodium phosphate (pH 7.1) and hemithioacetal (MG-SG) was pre-incubated for 20 min at 30 °C. Concentrations of MG and GSH were calculated and varied by using equation constant $Kd = 3.0$ mM to obtain desired concentration of MG-SG. Excess free GSH in the assay was kept at 0.10 mM. Reaction was initiated by addition of recombinant human His-GLO1 (3.0 nM) to the reaction buffer. Ki values of the inhibitors were evaluated by Dixon plot.

3. Results and discussion

To obtain the optimal docking configuration and scoring function for curcumin, the substrate HIPC-GSH was extracted from the X-ray structures of GLOI [4] and redocked it again into the same protein (self-docking) via a variety of docking conditions and scoring functions. CDOCKER was used to yield the closest model to the crystallographic structure. As a result, the RMSD between the optimal docked pose and the crystallographic one was 0.83 (Fig. S1 in the Supporting information), which confirmed that the docking protocol CDOCKER was reliable enough for this system. Subsequently, curcumin and bisdemethoxycurcumin were docked into the substrate-binding pocket of GLOI with the same optimal docking parameters and scoring function performed.

The crystallographic GLOI/HIPC-GSH complex was subjected to a 6 ns MD simulation procedure. After 3 ns MD simulations, the complex gave the RMSD values converged below 1.2 Å, which means the MD trajectories of the complex appear to be well equilibrated.

To validate the dynamic stability of the two GLOI/curcumin complexes, the RMSD for the backbone atoms along the 6 ns MD trajectories were monitored using the initial X-ray crystal structure as a reference. Fig. S2 gives the RMSD values of the two complexes converged below 2 Å, which means the MD trajectories of the two complexes appear to be well equilibrated. Therefore, the subsequent analyses are based on the MD trajectories truncated between 5 and 6 ns.

3.1. The binding models of the GLOI/curcumin complexes

To reveal the structural basis of the ligand-binding patterns for the two complexes, the average structures (Fig. 1) were generated by averaging 100 snapshots from the last 0.1 ns on the MD trajectory. The RMSD value between the keto and enol complexes is 1.05 Å as calculated by the corresponding aligned residues, which also verifies the accuracy of the modeled structures. Both structures were fitted to the X-ray crystal structure, and the RMSD values for the keto and enol complexes are 1.17 Å and 0.99 Å, respectively.

Fig. 2 gives the binding modes of the enol and keto forms of curcumin in the active site pocket of GLOI based on the above two average structures, while Fig. 3 displays how the enol form binds within the active site pocket of GLOI. The two figures can be used to elucidate the intermolecular interactions between curcumin and GLOI. According to Fig. 2A, the binding site for the enol form to GLOI consists of sixteen residues, that is His A126, Lys A156, Met A157, Phe A162, Glu A172, Met A179, Met A183, Gln B33, Cys B60, Phe B62, Met B65, Phe B67, Leu B69, Phe B71, Leu B92, and Glu B99. Due to the hydrophobic feature of curcumin, it is very reasonable to speculate
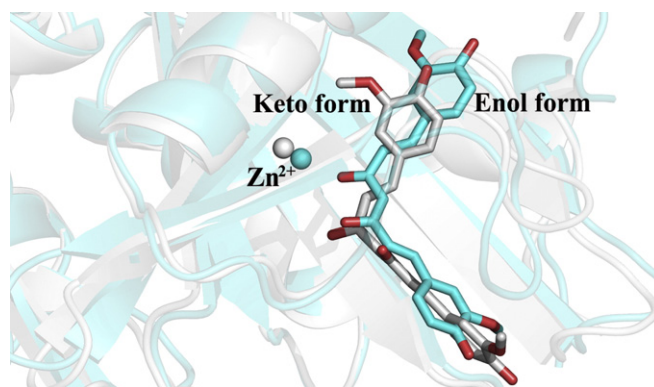

Fig. 1. The simulated structures of glyoxalase I in complexes with the enol and keto forms of curcumin. Glyoxalase I is shown in ribbon while curcumin is shown in CPK. The carbon atoms in the keto and enol forms are shown in grey and cyan, respectively, while the oxygen atoms are shown in red.
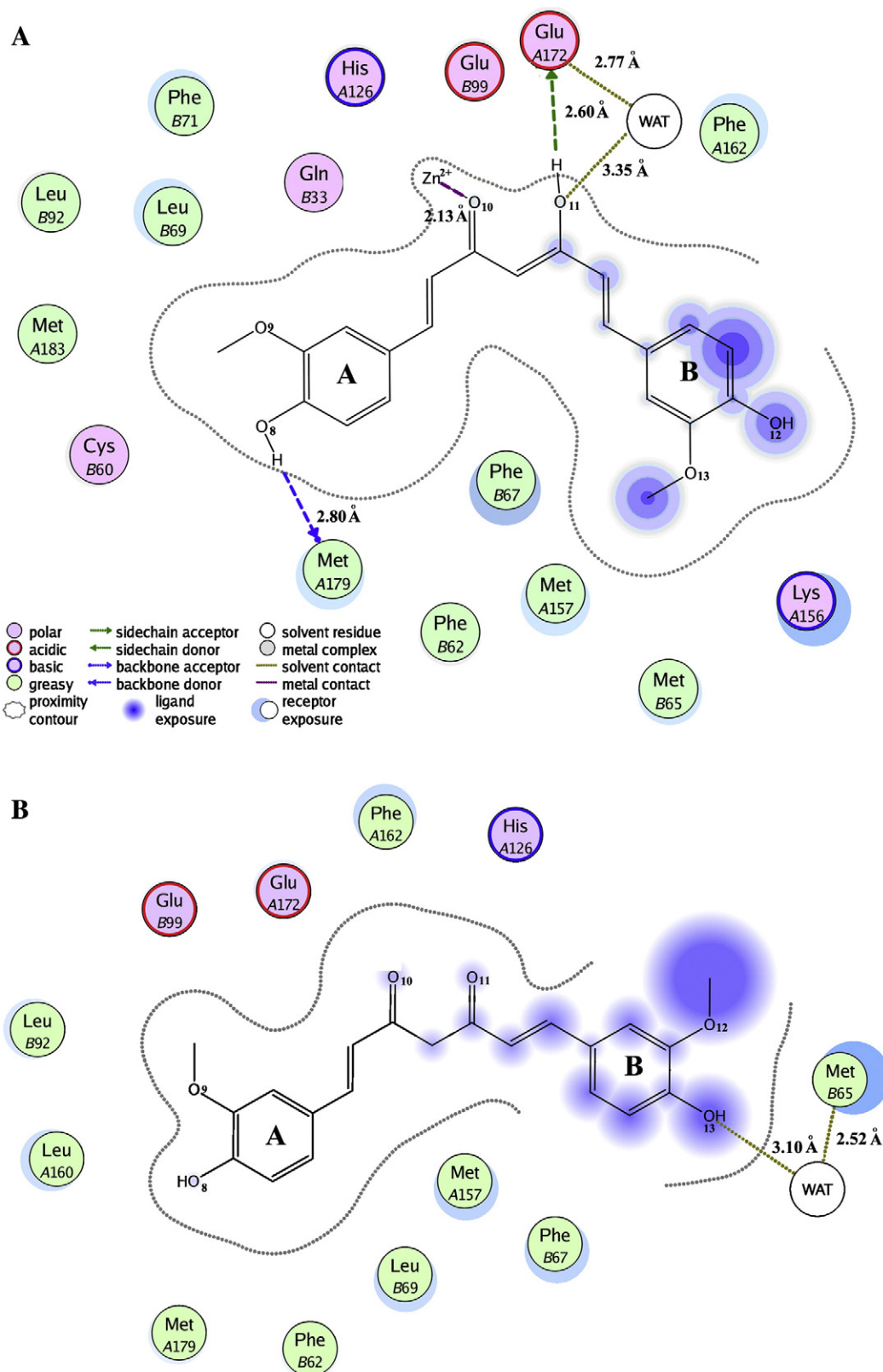
Fig. 2. The binding modes of the enol and keto forms of curcumin in the active site pocket of GLOI after 6 ns molecular dynamics simulations. A and B made with MOE are for the enol and keto forms, respectively, and elucidate the interactions between glyoxalase I and curcumin in the active site pocket.

that the hydrophobic interactions should play an important role in the binding of curcumin with GLOI. The ring A of curcumin is embraced by residues Met A179, Met A183, Cys B60, Leu B69 and Phe B71, which hold ring A closely in the hydrophobic pocket. Besides, the O_8 atom of

phenolic hydroxyl group forms a hydrogen bond (H1) of 2.80 Å with the O atom of Met A179. It could explain why the enol form can be buried deeper in the active site pocket of GLOI relative to the keto counterpart (Fig. 1).
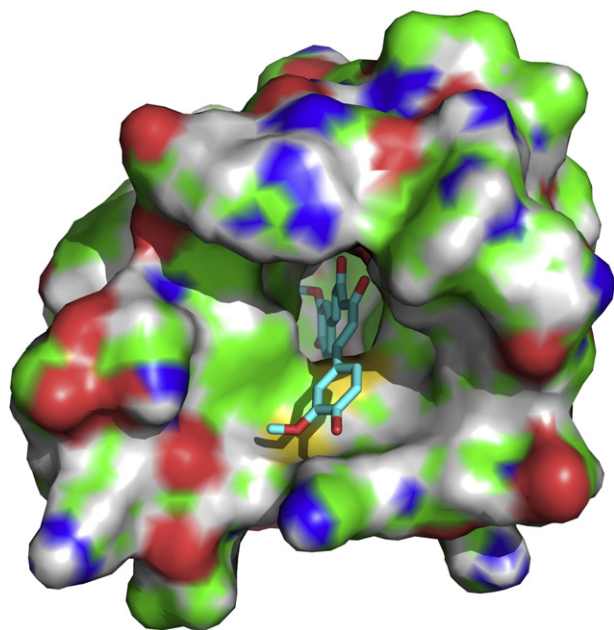
Fig. 3. The binding mode of the enol form of curcumin in glyoxalase I (carbon: cyan; oxygen: red). The active site pocket which is displayed as a water-accessible surface (probe diameter 1.4 Å) is defined as residues found within 8 Å range of curcumin.

The carbonyl and hydroxy group of the alkyl chain point to the zinc binding site. They are constricted in a plane with a distance of 2.79 Å between the two oxygen atoms. The carbonyl O_{10} atom forms a coordination bond of 2.13 Å with the zinc ion (the distance of the coordination bond is monitored in Fig. S3), which also contributes to the binding of curcumin within the active site pocket of GLOI. The hydroxyl O_{11} atom is within hydrogen bonding distance (H2 = 2.60 Å) of the OE2 atom of Glu A172. Furthermore, a water molecule entered the active site and contributes to the binding of curcumin with GLOI. A hydrogen bond (H3) of 3.35 Å is observed between the O atom of the water molecule and the O_{11} atom of curcumin. In addition, the water molecule forms a hydrogen bond (H4) to the closet residue Glu A172. The distances of H3 and H4 are monitored in Fig. S4. It is clear that H4 is more stable than H3. The ring B forms van der Waals' interactions with residues Met B65, Phe B67, and Met A157. As a result, these energetically favorable interactions stabilize the enol form of curcumin in the active site pocket.

The keto form of curcumin exhibits a weak interaction with GLOI. The keto form processes a symmetry structure, however, because of the electrostatic exclusion of the two carbonyl groups, the rotatable bonds between them cause the two antimeric parts to set up a torsion about 90°. The hydroxyl O_{11} atom of the enol form can form a strong hydrogen bond with Glu A172, in contrast, the carbonyl group at the same position of the keto counterpart exhibits the unfavorable electrostatic repulsion with Glu A172 and Glu B99. As a result, either of the two carbonyl groups is not within coordination distance of the zinc ion. As shown in Fig. S3, the distance between the carbonyl O_{10} atom of the keto form and the zinc ion fluctuates around 5 Å during the 6 ns MD simulations. Thus, curcumin was pushed away toward the opening of the active site pocket. And the side chain of Glu A172 rotated about 30° to make another coordination bond with the zinc ion instead. The ring A is placed in the binding pocket consisted of residues Met A157, Leu A160, Leu A162, Met A179, Phe B62, Glu B69, and Leu B92.

Interacting with the zinc ion is a crucial element of binding for GLOI. The two forms disagree only in a small part, however result in dramatic differences in the binding modes. The main cause is that the enol form can form a stable coordination bond with the zinc ion, and the keto

counterpart fails to have a close contact with the zinc ion. In addition, the enol tautomer penetrates deeper into in the active site of GLOI, and forms at least two hydrogen bonds with GLOI, whereas the keto counterpart does not make a hydrogen bond contact with the enzyme.

3.2. Comparison with the crystal structure of GLOI

HIPC-GSH is a transition state analogue mimicking the enediolate intermediate in the reaction pathway of GLOI and serves as a tight binding competitive inhibitor of human GLOI ($Ki = 10$ nM) [4]. However, curcumin processes a completely different backbone structure comparing with the intermediate analogues. It would be a fresh research direction for a new kind of GLOI inhibitors. So it's meaningful to compare the enol complex with the crystal structure in complex with HIPC-GSH to see the structural changes.

As shown in Fig. 4, the ring A of the enol form is 2.2 Å deeper in the hydrophobic pocket relative to the indophenol part of HIPC-GSH in the crystal structure. There are two reasons for that. One is that the O_8 atom of phenol group forms a hydrogen bond (H1) of 2.80 Å with the O atom of Met A179 (Fig. 2). The other is that the carbonyl O atom of the enol form is almost overlapped with the OZ_1 atom of HIPC-GSH, indicating the similarity of the two ligands coordinating with the zinc ions. The carbonyl group of the enol form is attracted to zinc within the coordinate position so that the whole molecule is inducted into the deeper site.

An important flexible loop including residues 152–159 over the active site was described in the previous study [4]. It was proposed that the loop was open in the absence of a bound ligand to allow the substrate to enter the active site. Once HIPC-GSH binded to GLOI, the main chain nitrogens of Met A157 and Lys A156 moved down into the active site to form hydrogen bonds with the carboxylate oxygens of the glycine moiety, then closed the loop over the ligand, which strongly constrained the mobility of the loop. The O_{12}/O_{13} atoms of the enol tautomer could possibly form hydrogen bonds with the NZ atom in the side chain of Lys A156. According to the MD results (Fig. S5), the O_{13} atom of curcumin partially remains within hydrogen bond distance to the NZ atom of Lys A156. Thus, the flexible loop could not be fully stabilized by curcumin, which might be one of the reasons why curcumin only has a moderate activity.

3.3. Binding-free-energy calculations and enzyme kinetics analysis

According to the quantum mechanics calculations at the B3LYP/6-311G* level and experiments done by T. M. Kolev, the enol form of
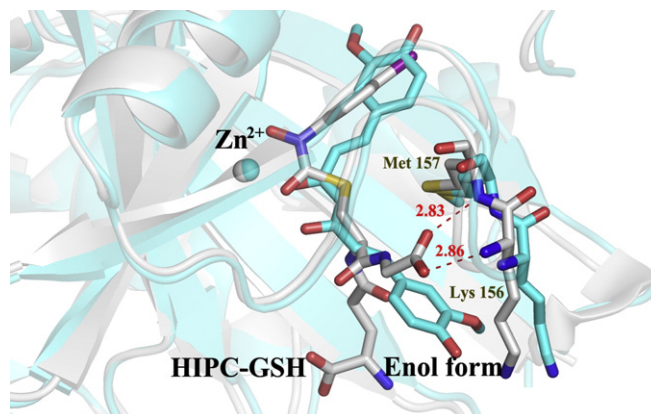

Fig. 4. The comparison between the crystal structure of glyoxalase I in complex with HIPC-GSH [4] and the simulated structure of glyoxalase I plus the enol form of curcumin. The carbon atoms in the crystal structure and the enol complex are shown in grey and cyan, respectively. The red numbers indicate the length of two hydrogen bonds between glyoxalase I and HIPC-GSH in Å.

Table 1
Components of the binding free energies of calculated from their trajectories (kcal/mol).

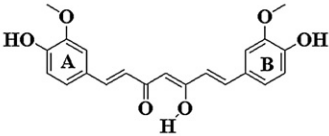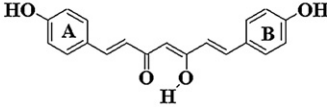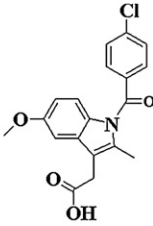| Energy terms	Glyoxalase I + enol form of curcumin		Glyoxalase I + keto form of curcumin		Glyoxalase I + bisdemethoxycurcumin	
	Mean	Std.	Mean	Std.	Mean	Std.
ΔG_{ele}	− 54.47	8.42	− 10.80	2.95	− 48.87	7.80
ΔG_{vdW}	− 33.48	4.07	− 39.38	2.36	− 28.15	4.06
$\Delta G_{ele,sol}$	63.73	5.71	31.39	2.82	54.80	3.88
$\Delta G_{nonpol,sol}$	− 6.15	0.16	− 5.36	0.18	− 5.18	0.12
ΔG_{MM}	− 87.96	7.38	− 50.18	3.59	− 77.02	5.93
ΔG_{sol}	57.57	5.65	26.03	2.77	49.62	3.86
ΔG_{bind}	− 30.38	3.92	− 24.16	2.46	− 27.40	3.68

ΔG_{ele} are electrostatic interactions calculated by the MM force field.
ΔG_{vdW} are van der Waals contributions from MM.
$\Delta G_{ele,sol}$ are the polar contribution to solvation.
$\Delta G_{nonpol,sol}$ are the nonpolar contribution to solvation.
$\Delta G_{MM} = \Delta G_{ele} + \Delta G_{vdw}$ and $\Delta G_{sol} = \Delta G_{ele} + \Delta G_{vdw}$.
ΔG_{bind} are binding free energies in the absence of entropic contribution.

curcumin is more stable than the keto counterpart in the water [14]. To obtain further information of the curcumin/GLOI interactions in the two systems, the binding-free-energy calculations using the MM-PBSA method were performed. Table 1 lists calculated binding free energies (ΔG_{bind}), averaged over 500 snapshots for three simulations. According to Table 1, a less negative value of ΔG_{bind} (− 24.16 kcal/mol) for the keto complex than that for the enol complex ($\Delta G_{bind} = −30.38$ kcal/mol) corresponds a decrease in the binding affinity. The difference in the calculated binding free energies between the two complexes is 6.22 kcal/mol. Consequently, our energetic results suggests that GLOI prefers the enol form of curcumin to the keto tautomer, which implies that the enol form exhibits a stronger potency of binding to GLOI than the keto counterpart, and the former is more important for the intermolecular interactions with GLOI. Our energetic analyses reveal that electrostatic and van der Waals energies are the major contributions to the binding of the enol form with GLOI, whereas the polar energies oppose the binding, which is common in the literature [30,32,35,36]. In the binding mode of the enol form, coordination bond, hydrogen bond, and van der Waals interactions are primarily considered to contribution to the binding free energy.

A curcumin analogue bisdemethoxycurcumin (Fig. 5) was subjected to identical molecular modeling procedures. Based on our MD results, the enol form of bisdemethoxycurcumin can bind to GLO in a similar manner as curcumin. Its calculated binding free energy is − 27.40 kcal/mol and is slightly less negative than that of curcumin, which corresponds to a decrease in the inhibitory ability. The structural analysis revealed that the binding mode of bisdemethoxycurcumin to GLOI is quite similar to that of enol form of curcumin. The O_8 atom of phenolic hydroxyl group in bisdimethoxycurcumin forms a hydrogen bond of 2.97 Å with the O atom of Met A179, but which is longer than that (2.80 Å) in the enol complex. In addition, the absence of two methoxy groups leads to a decrease of ΔG_{vdW}. The weaker H-bond interaction and the reduction of van der Waals interactions could explain why bisdimethoxycurcumin binds less strongly to the enzyme than curcumin.

Our kinetic analysis showed that curcumin, bisdemethoxycurcumin, and indomethacin (an inhibitor of GLOI) exhibit a competitive-type inhibition pattern. The experimental Ki values for curcumin, bisdemethoxycurcumin, and indomethacin against GLOI are 10.3 ± 0.5, 18.2 ± 0.8, and 24.4 ± 1.5 μM (Fig. 5 and S6), respectively. Previously reported Ki values of curcumin and indomethacin were 5.1 and 18.1 μM [13,37], respectively. $\Delta G_{bind,exp}$ was estimated approximately from Ki via $\Delta G \approx −RT\ln(Ki)$ for direct comparison. The $\Delta G_{bind,exp}$ for curcumin and bisdemethoxycurcumin are − 6.82 and − 6.48 kcal/mol, respectively. Since entropic contribution ($T\triangle S$) was excluded, the calculated binding free energies were more negative than these estimated from the experimental Ki values. However, it was still of significance to compare their relative magnitude. The increasing order in our experimental Ki values (curcumin and bisdemethoxycurcumin) is consistent with our

Calculated binding free energy (kcal/mol)	**-30.38**	**-27.40**	—
Ki (μM)	10.3 ± 0.5	18.2 ± 0.8	24.4 ± 1.5
Ki (μM)*	5.1	—	18.1

*The Ki values in the literature [13,38].

Fig. 5. The experimental Ki values and structures of curcumin, bisdemethoxycurcumin, and indomethacin.

computational results, which indicates that MD simulations and binding-free-energy calculations can provide an alternative way to evaluate the inhibitory ability against GLOI.

4. Conclusion

The present study provides a structural insight into the curcumin-bound patterns to GLOI. The calculated binding free energies for the keto and enol complexes are −24.16 and −30.38 kcal/mol, respectively, indicating that the enol form of curcumin is more potential for the binding with GLOI. The carbonyl O_{10} atom of the enol tautomer coordinates with the zinc ion specifically, however, the keto counterpart does not coordinate with the zinc atom since it displays unfavorable electrostatic interactions with Glu A172 and Glu B99. Both the binding mode and calculated binding free energy demonstrate that the primary enol form can directly inhibit GLOI, and cause the physiological effect.

The O_{13} atom of curcumin partially remains to form hydrogen bond with the NZ atom of Lys A156. Thus, the flexible loop including residues 152–159 over the active site could not be fully stabilized by curcumin, which could account for why curcumin only has a moderate inhibitory activity against GLOI.

Our modeling studies reveal that bisdemethoxycurcumin binds to GLOI in a similar manner as curcumin and exhibits a weaker predicted binding free energy, which is validated by our kinetic analysis. Our results indicate that the MD simulations and binding-free-energy calculations can provide an alternative way to evaluate the inhibitory ability against GLOI and help the development of novel GLOI inhibitors. The current MD simulation and MM-GBSA approaches would be useful for the exploratory study of some biological systems for drug discovery purpose, especially for cases difficult to obtain the crystal structure of a receptor/ligand complex.

Acknowledgements

Appendix A. Supplementary data

Supplementary data associated with this article can be found, in the online version, at doi: 10.1016/j.bpc.2009.12.007.

References

[1] P.K. Padmanabhan, A. Mukherjee, R. Madhubala, Characterization of the gene encoding glyoxalase II from *Leishmania donovani*: a potential target for anti-parasite drugs, Biochem. J. 393 (2006) 227–234.

[2] P.J. Thornalley, The glyoxalase system: new developments towards functional characterization of a metabolic pathway fundamental to biological life, Biochem. J. 269 (1990) 1–11.

[3] P.J. Thornalley, L.G. Edwards, Y. Kang, C. Wyatt, N. Davies, M.J. Ladan, J. Double, Antitumour activity of S-p-bromobenzylglutathione cyclopentyl diester in vitro and in vivo: inhibition of glyoxalase I and induction of apoptosis, Biochem. Pharmacol. 51 (1996) 1365–1372.

[4] A.D. Cameron, M. Ridderstrom, B. Olin, M.J. Kavarana, D.J. Creighton, B. Mannervik, Reaction mechanism of Glyoxalase I explored by an X-ray crystallographic analysis of the human enzyme in complex with a transition state analogue, Biochemistry 38 (1999) 13480–13490.

[5] R. Vince, S. Daluge, Glyoxalase inhibitors. A possible approach to anticancer agents, J. Med. Chem. 14 (1971) 35–37.

[6] M.L. Clapper, S.J. Hoffman, K.D. Tew, Glutathione S-transferases in normal and malignant human colon tissue, Biochim. Biophys. Acta 1096 (1991) 209–216.

[7] F.M. Ayoub, R.E. Allen, P.J. Thornalley, Inhibition of proliferation of human leukaemia 60 cells by methylglyoxal in vitro, Leuk. Res. 17 (1993) 397–401.

[8] L.G. Egyud, A. Szent-Gyorgyi, Cancerostatic action of methylglyoxal, Science 160 (1968) 1140.

[9] E.M. Sharkey, H.B. O'Neill, M.J. Kavarana, H. Wang, D.J. Creighton, D.L. Sentz, J.L. Eiseman, Pharmacokinetics and antitumor properties in tumor-bearing mice of an enediol analogue inhibitor of glyoxalase I, Cancer Chemother. Pharmacol. 46 (2000) 156–166.

[10] A. Kalsi, M.J. Kavarana, T. Lu, D.L. Whalen, D.S. Hamiton, D.J. Creighton, Role of hydrophobic interactions in binding S-(N-Aryl/Alkyl- N-hydroxycarbamoyl) glutathiones to the active site of the antitumor target enzyme glyoxalase I, J. Med. Chem. 43 (2000) 3981–3986.

[11] D.J. Creighton, Z.-B. Zheng, R. Holewinski, D.S. Hamilton, J.L. Eiseman, Glyoxalase I inhibitors in cancer chemotherapy, Biochem. Soc. T. 31 (2003) 1378–1382.

[12] A. Goel, A.B. Kunnumakkara, B.B. Aggarwal, Curcumin as "Curecumin": from kitchen to clinic, Biochem. Pharmacol. 75 (2008) 787–809.

[13] T. Santel, G. Pflug, N.Y.A. Hemdan, A. Schäfer, M. Hollenbach, et al., Curcumin inhibits glyoxalase 1—a possible link to its anti-inflammatory and anti-tumor activity, PLoS ONE 3 (2008) e3508–e3513.

[14] T.M. Kolev, E.A. Velcheva, B.A. Stamboliyska, M. Spiteller, DFT and experimental studies of the structure and vibrational spectra of curcumin, Int. J. Quantum. Chem. 102 (2005) 1069–1079.

[15] R. Takasawa, S. Takahashi, K. Saeki, S. Sunaga, A. Yoshimoria, S. Tanumaa, Structure–activity relationship of human glyoxalase I inhibitory natural flavonoids and their growth inhibitory effects, Bioorgan. Med. Chem. 16 (2008) 3969–3975.

[16] E. Skrzypczak-Jankun, N.P. McCabe, S.H. Selman SH, J. Jankun, Int. J. Mol. Med. 5 (2000) 521–526;
E. Skrzypczak-Jankun, K.J. Zhou, N.P. McCabe, S.H. Selman, J. Jankun, Structure of curcumin in complex with lipoxygenase and its significance in cancer, Int. J. Mol. Med. 12 (2003) 17–24.

[17] Accelrys Software Inc., Accelrys Discovery Studio 2.1, San Diego, 2008.

[18] G. Wu, D.H. Robertson, C.L. Brooks, M. Vieth, Detailed analysis of grid-based molecular docking: a case study of CDOCKER-A CHARMm-based MD docking algorithm, J. Comp. Chem. 24 (2003) 1549–1562.

[19] D.A. Case, T.A. Darden, T.E. Cheatham III, C.L. Simmerling, J. Wang, et al., AMBER 10, University of California, San Francisco, 2008.

[20] M.J. Frisch, G.W. Trucks, H.B. Schlegel, G.E. Scuseria, M.A. Robb, et al., Gaussian 03, Revision E.01, Gaussian, Inc, Pittsburgh PA, 2004.

[21] J.M. Wang, W. Wang, P.A. Kollman, Antechamber: an accessory software package for molecular mechanical calculations, J. Am. Chem. Soc. 222 (2001) U403 Abstr.

[22] J. Aqvist, A. Warshel, Computer simulation of the initial proton transfer step in human carbonic anhydrase I, J. Mol. Biol. 224 (1992) 7–14.

[23] Z.R. Wasserman, C.N. Hodge, Fitting an inhibitor into the active site of thermolysin: a molecular dynamics case study, Proteins 24 (1996) 227–237.

[24] R.H. Stote, M. Karplus, Zinc binding in proteins and solution: a simple but accurate nonbonded representation, Proteins 23 (1995) 12–31.

[25] H.J.C. Berendsen, J.P.M. Postma, W.F. van Gunsteren, A. DiNola, J.R. Haak, Molecular dynamics with coupling to an external bath, J. Chem. Phys. 81 (1984) 3684–3690.

[26] S. Miyamoto, P.A. Kollman, Settle: an analytical version of the SHAKE and RATTLE algorithm for rigid water models, J. Comput. Chem. 13 (1992) 8952–8962.

[27] T. Darden, D. York, L. Pedersen, Particle mesh Ewald: an N · log(N) method for Ewald sums in large systems, J. Chem. Phys. 98 (1993) 10089–10092.

[28] F. Fogolari, A. Brigo, H. Molinari, Protocol for MM/PBSA molecular dynamics simulations of proteins, Biophys. J. 85 (2003) 159–166.

[29] P.A. Kollman, I. Massova, C. Reyes, B. Kuhn, S. Huo, M. Lee, T. Lee, Y. Duan, W. Wang, O. Donini, P. Cieplak, J. Srinivasan, D.A. Case, T.E. Cheatham, Calculating structures and free energies of complex molecules: combining molecular mechanics and continuum models, Acc. Chem. Res. 33 (2000) 889–897.

[30] J. Zeng, W.H. Li, Y.X. Zhao, G.X. Liu, Y. Tang, H.L. Jiang, Insights into ligand selectivity in estrogen receptor isoforms: molecular dynamics simulations and binding free energy calculations, J. Phys. Chem. B 112 (2008) 2719–2726.

[31] W.C. Still, A. Tempczyk, R.C. Hawley, T. Hendrickson, Semianalytical treatment of solvation for molecular mechanics and dynamics, J. Am. Chem. Soc. 112 (1990) 6127–6129.

[32] M.F. Sanner, A.J. Olson, J.-C. Spehner, Reduced surface: an efficient way to compute molecular surfaces, Biopolymers 38 (1996) 305–320.

[33] S.B. Nolde, A.S. Arseniev, V.Y. Orekhov, M. Billeter, Essential domain motions in barnase revealed by MD simulations, Proteins 46 (2002) 250–258.

[34] M. Kawatani, H. Okumura, K. Honda, N. Kanoh, M. Muroi, N. Dohmae, M. Takami, M. Kitagawa, Y. Futamura, M. Imoto, H. Osada, The identification of an osteoclastogenesis inhibitor through the inhibition of glyoxalase I, P. Natl. Acad. Sci. (USA) 105 (2009) 11691–11696.

[35] R. Chachra, R.C. Rizzo, Origins of resistance conferred by the R292K neuraminidase mutation via molecular dynamics and free energy calculations, J. Chem. Theory Comput. 4 (2008) 1526–1540.

[36] F.M. Ruiz, R. Gil-Redondo, A. Morreale, A.R. Ortiz, C. Fabrega, J. Bravo, Structure-based discovery of novel non-nucleosidic DNA alkyltransferase inhibitors: virtual screening and in vitro and in vivo activities, J. Chem. Inf. Model. 48 (2008) 844–854.

[37] S. Sato, Y. Kwon, S. Kamisuki, N. Srivastava, Q. Mao, Y. Kawazoe, M. Uesugi, Polyproline-rod approach to isolating protein targets of bioactive small molecules: isolation of a new target of indomethacin, J. Am. Chem. Soc. 129 (2007) 873–880.